The structure of lead-silicate glasses: molecular dynamics and EXAFS studies

2001 J. Phys.: Condens. Matter 13 9781

(http://iopscience.iop.org/0953-8984/13/43/309)

INSTITUTE OF PHYSICS PUBLISHING JOURNAL OF PHYSICS: CONDENSED MATTER

J. Phys.: Condens. Matter **13** (2001) 9781–9797 PII: S0953-8984(01)24005-3

The structure of lead-silicate glasses: molecular dynamics and EXAFS studies

Jarosław Rybicki[1,3], Anna Rybicka[1], Agnieszka Witkowska[1,3], Grzegorz Bergmański[1], Andrea Di Cicco[2], Marco Minicucci[2] and Giorgio Mancini[2]

[1] Department of Solid State Physics, Faculty of Technical Physics and Applied Mathematics, Technical University of Gdansk, Narutowicza 11/12, 80-952 Gdansk, Poland
[2] INFM, Department of Mathematics and Physics, University of Camerino, Madonna delle Carceri, Camerino (MC), Italy

Received 13 April 2001, in final form 3 August 2001
Published 12 October 2001
Online at stacks.iop.org/JPhysCM/13/9781

Abstract

Molecular dynamics (MD) simulations and extended x-ray absorption fine structure (EXAFS) investigations of the structure of lead-silicate glasses, $x\mathrm{PbO}(1-x)\mathrm{SiO_2}$, have been undertaken to elucidate the problem of partially contradicting experimental findings reported in the literature about basic structural units and their interconnection. The MD simulations were performed in a wide range of compositions, $x = 0.1$–0.9. The atoms were assumed to interact by a two-body Born–Mayer–Huggins interaction potential. The EXAFS measurements were performed for $x = 0.3$, 0.5 and 0.7, and also for pure crystalline (red) PbO at the L_3-edge of Pb. The absorption spectra were analysed within the GNXAS approach.

Our EXAFS and MD results are in good agreement, and support some previous suggestions that: (1) the PbO_4 groups are the dominant structural units in lead-silicate glasses for any concentration and (2) at lower PbO concentrations the co-existence of the PbO_4 and PbO_3 groups is possible.

The medium-range ordering in the simulated glasses has also been investigated in detail. The connectivity of the SiO_4 tetrahedra network breaks at about $x = 0.45$, whereas the Pb structural units form a continuous (mainly edge-sharing) network even at relatively low PbO concentrations ($x > 0.2$). The cation–anion ring statistics is also discussed.

1. Introduction

Lead-silicate glasses find a lot of industrial applications, mainly as optical glasses [1]. They are used as special materials in electronics and optoelectronics in the production of image plate

[3] Also at: TASK Computer Centre, Narutowicza 11/12, 80-952 Gdansk, Poland.

amplifiers and scintillators [2]. Modified lead-silicate glasses, containing metallic Pb granules, reveal a high secondary emission coefficient, and thus find application in the production of electron channel multipliers [3].

The atomic structure of the lead-silicate glasses has been investigated for sixty years. Various experimental techniques have been used, such as IR spectroscopy [4], Raman spectroscopy [4–6], NMR [5, 7, 8], XPS [9], x-ray diffraction [10, 11], neutron diffraction methods [12, 13], extended x-ray absorption fine structure (EXAFS) and x-ray absorption near-edge structure (XANES) [8, 14]. However, until now, no single, commonly accepted structural model for $x\mathrm{PbO}(1-x)\mathrm{SiO}_2$ glasses has been elaborated. It is still not clear how the structural parameters change with variations of x. For these reasons we performed extensive molecular dynamics (MD) [15, 16] investigations of the considered glasses in the whole range of glass formation, and EXAFS [17–19] measurements for several chosen glass compositions. Some results of our previous preliminary MD simulations of the considered systems were described briefly in [20, 21]. The results reported briefly in [20] were obtained at extremely high cooling rates for very small samples and no deeper structural analysis has been performed. The results contained in [21] refer to one glass composition only (PbO content $x = 0.1$).

EXAFS appears to be the most suitable technique to study the short-range structure around lead atoms in the multi-component glasses. The local partial Pb–O pair distribution function can be reliably reconstructed [22] by EXAFS experiments using advanced techniques [18, 19], and compared with models of short-range ordering provided by MD [23, 24]. If a good agreement between the EXAFS and MD results on the short-range ordering is found, and at the same time the potential parametrization used in the simulations allows correct system density to be obtained, one can expect that the medium-range ordering in the MD-simulated structure should be rather reliable. Thus, using EXAFS and MD methods simultaneously, one can also get some insight into the medium-range order in the considered systems. In this paper we apply the mentioned strategy in order to extract information on the medium-range order in our glasses. In particular, the cation–anion rings' analysis of the MD-simulated structures [25–29] was performed.

This paper is organized as follows. Section 2 is dedicated to several rather technical issues, such as some details on the simulation method, sample preparation and the EXAFS measurements. In section 3 we describe the short range ordering around the lead atom, and in sections 3.1 and 3.2 we present our MD and EXAFS results, respectively. In sections 3.3 and 3.4 we compare our data with the previous results of other authors. In section 4 we discuss the medium-range order viewed by MD calculations. Section 5 contains concluding remarks.

2. Numerical simulations and experiment—technical issues

2.1. Molecular dynamics simulations

The molecular dynamics (MD) simulations have been performed in the (NpH) ensemble [30]. The atoms, placed in a cubic simulation box with periodic boundary conditions, interacted by two-body forces: the Born–Mayer repulsive forces and Coulomb forces due to full ionic charges, calculated with the aid of the standard Ewald technique [16], which is suitable also for disordered systems. However, the summation method convergence can be worse than in crystals. Thus, special care must be taken in choosing the values of the summation range $k_{\max}$ in the reciprocal space of the α-parameter determining the convergence in real space and of the cut-off radius for the calculation of the short range interactions. The proper determination of these parameters and the error analysis were described in detail in [31], and in our simulations we have taken into account the experiences reported therein. The potential parametrization was

Table 1. The numbers of atoms in the cubic simulation box and the box edge lengths L for all glass compositions.

x	Pb	Si	O	L (Å)
0.10	100	900	1900	35.8
0.20	200	800	1800	35.5
0.25	200	600	1400	32.8
0.33	400	800	2000	37.4
0.40	500	750	2000	37.1
0.45	540	660	1860	36.4
0.50	500	500	1500	34.2
0.67	800	400	1600	28.2
0.80	800	200	1200	32.9
0.90	900	100	1100	33.1

taken from [32]. This potential allowed us to perform successfully the MD simulations at zero external pressure over a wide range of compositions, leading to equilibrium densities close to the experimental values and reasonable thermo-mechanical coefficients [33]. All the systems discussed in the present work were initially prepared in a well-equilibrated molten state at 10 000 K, and then slowly cooled down to 300 K, passing equilibrium states at 8000 K, 6000 K, 5000 K, 4000 K, 3000 K, 2500 K, 2000 K, 1500 K, 1000 K and 600 K. At each temperature the system was equilibrated during 30 000 fs time steps, and then sampled during 10 000 fs time steps. During the equilibration runs, a velocity scaling was applied whenever the rolling average of the temperature (calculated over last 100 time steps) went out from the interval $(T - \Delta T, T + \Delta T)$, using $\Delta T = 100$ K for $T \geqslant 1000$ K, and $\Delta T = 20$ K and $\Delta T = 10$ K for $T = 600$ K and $T = 300$ K, respectively. Such a run scheme corresponds to the average cooling rate of 2×10^{13} K s^{-1}.

The simulations have been performed in the whole range of glass formation, i.e. for $0.0 \leqslant x \leqslant 0.9$. Depending on the glass stoichiometry, the number of atoms within the simulation box ranged from 1600 to 3250 (see table 1 for details), resulting in box-edge lengths of 28–36 Å.

The structural information on short-range correlation was obtained in a conventional way, mainly from radial and angular distribution functions. The medium-range order was studied mainly via cation–anion ring analysis, performed using our new program package ANELLI [27–29]. In this package, a highly efficient algorithm for ring perception is implemented. The algorithm follows the general guidelines of Balducci and Pearlman's message passing method [34], but a new method based on a pre-filtering technique is introduced to perceive rings in structures represented by 2-connected graphs [25, 26]. Our approach enforces full ring formation (i.e. a ring of length n is assured to close on each of its n nodes leading to n equal rings), so that, once detected and processed for linear independence, all n-sized rings closing on a node N and all n-sized rings closing on a different node M, and including node N, can be safely regarded and ignored as copies of rings previously processed. While allowing for full ring formation, redundancy from collapsing paths (i.e. paths closing on their originating node) and of different type not related to full ring formation is monitored and prohibited from propagation.

2.2. Sample preparation

Lead-silicate glasses of composition $x\mathrm{PbO}(1 - x)\mathrm{SiO_2}$ (% mol), $x = 0.3$, 0.5, 0.7 were synthesized as follows. Mixtures of powdered oxides, placed into a platinum crucible

were submitted to gradual heating in an electric furnace from room temperature to melting temperature. For our compositions the temperature ranged from 1100 °C for $x = 0.7$ to 1350 °C for $x = 0.3$. The melts were kept at their melting temperature for a few minutes and were mechanically stirred in order to homogenize the whole melt volume. The melts were quenched by pouring them on a brass plate. The samples obtained in such a way were transparent and had a uniform colour. True glassy structure of the samples was confirmed by the absence of Bragg peaks in the x-ray diffraction patterns. The pieces of the prepared glasses were milled. The average diameter of grains amounted to about 20 μm. Next, the proper amounts of the powdered glasses were mixed with an inert matrix powder (in this case BN, boron nitride 99%) at weight ratio 1:10 or 1:15. Finally the mixtures were pressed into pellets of typical thicknesses of 0.5–1 mm.

2.3. XAS measurements

X-ray absorption spectroscopy (XAS) spectra of the lead-silicate glasses at the Pb L_3-edge have been recorded at the BM29 beam-line at the European Synchrotron Radiation Facility (Grenoble) using a double-crystal monochromator equipped with a Si(3 1 1) crystals with an average resolution in the whole range of energy around 1.5 eV (FWHM), (0.3 mm vertical slit). The spectra of pure PbO at the Pb L_3-edge have been collected at the D42 beam-line at the LURE laboratories (Orsay, Paris), equipped with a Si(3 3 1) channel-cut monochromator (average resolution of about 2.5 eV). The DCI storage ring was operating at 1.85 GeV with typical currents of about 300 mA. The measurements were performed at room temperature. The spectra were recorded with variable energy step over the total energy range 12 900–14 000 eV (the Pb L_3-edge energy is 13 035 eV). The sampling steps were equal to 3.0 eV and 0.4 eV in the energy ranges 12 900–13 000 eV and 13 000–13 100 eV, respectively. In the range between 13 100 and 14 000 eV the sampling step was increased from 0.4 to 2 eV. The step reproducibility of the BM29 monochromator is better than 0.1 eV. This scanning procedure yielded high quality data of both pre- and post-edge background analyses used for normalization of the spectra. The pre-edge region was fitted linearly, whereas the post-edge background was approximated by a spline function. XANES spectra were normalized by subtracting the pre-edge background from all points, and dividing the difference by the absorption jump. The EXAFS experimental data have been analysed with advanced data-analysis techniques, using theoretical calculation of the x-ray absorption cross section in the framework of the GNXAS method (GN stands for the n-body distribution function in condensed matter, XAS denotes x-ray absorption spectroscopy) (for details see [18, 19]).

2.4. The method of EXAFS data analysis

The main characteristic of the GNXAS method [18, 19] is the possibility to calculate and perform the configurational average of multiple-scattering contributions (at any order) associated with two-, three- and four-atom configurations. This is accomplished by a continued fraction expansion algorithm [18, 19]. This method is appropriate for the study of disordered materials, since it correlates the spectra with the n-body distribution function g_n in a direct way. The local atomic arrangement around the absorber (0) is decomposed into irreducible atomic configurations containing only $2, 3, \ldots, n$ atoms, i.e. $\gamma^{(2)}(0, i)$, $\gamma^{(3)}(0, i, j)$, $\ldots$, $\gamma^{(n)}(0, i, j, \ldots, n-1)$. In our analysis only the two-body term $\gamma^{(2)}(0, i)$ expressed as the sum of multiple-scattering contributions $\chi_2(0, i, 0)$ and $\chi_4(0, i, 0, i, 0)$ was used. Other MS contributions and signals associated with three-body configurations were beyond the sensitivity of the EXAFS method in the case of the considered materials.

In addition, the GNXAS scheme can account for multi-electron excitation channels, affecting the modelling of the atomic backgrounds. The importance of taking double-electron excitations into account has been widely emphasized in several recent papers (see references [35–37] containing useful list of references on the subject). Inaccurate extraction of the atomic background neglecting double-electron channels can result in the presence of low-frequency components without structural origin in the EXAFS signal. The main effect on the structural parameters is a modification of the coordination number and/or of the mean-square relative displacement up to 10% and change of the average distance by about 1% [38]. Moreover, the quality of the fit largely decreases (by one order of magnitude or more).

Calculation of the XAS $\gamma^{(n)}$ signal is performed using an accurate complex energy-dependent self-energy function, which automatically accounts for the inelastic mean-free-path (MFP) of the excited photoelectron and for the core-hole lifetime [39]. In the present case the initial structure for phase shift calculation was pure red lead oxide (cluster of 8 Å radius) [40]. Phase shifts and structural signals associated with the first coordination shell have been calculated using PHAGEN and GNXAS codes, respectively (see [37] for a detailed description of the GNXAS package). The FITHEO program [37] has been used to perform fits of model absorption signal, composed of an appropriate background and the structural oscillation calculated for a chosen structural model, to the experimental EXAFS spectra in the energy space. The total number of refined structural parameters was four (first shell parameters R, σ^2, β, and N will be explained in section 3.1).

The amplitude reduction factor, S_o^2, which takes into account intrinsic inelastic processes, was kept within the estimated range (0.75 ± 0.01) for all the analysed samples. This range of S_o^2 variations was obtained from the best fitting between the theoretical and experimental EXAFS signal of the Pb crystal with a fixed value of a standard deviation for the first shell, $\sigma^2 \approx 0.0276$ Å^2, taken from MD simulations [41].

3. Short-range order

Let us discuss in turn the average short-range structure obtained by MD simulations (section 3.1), and by EXAFS experiment (section 3.2). Then, our numerical and experimental data are compared (section 3.3), and related to the results of other authors (section 3.4).

3.1. MD simulation results

The main feature of partial pair distribution functions (PDFs) is the first peak representing the first-neighbour coordination shell. As it has been shown in several recent papers, the PDFs in disordered systems can be decomposed in a short-range peak of a well-defined shape and a long-range tail [22, 23]. A simple Gaussian shape of the short-range peak of PDF is usually insufficient to describe accurately the short-range ordering in highly disordered systems. A useful parametrization of the first PDF peak, as shown previously [23, 42], has the form

$$p(r) = \frac{2}{\sigma\,|\beta|\,\Gamma\left(4/\beta^2\right)}\left(\frac{4}{\beta^2}+\frac{2\,(r-R)}{\sigma\beta}\right)^{\frac{4}{\beta^2}-1}\exp\left[-\left(\frac{4}{\beta^2}+\frac{2\,(r-R)}{\sigma\beta}\right)\right] \tag{1}$$

where $g(r)$ is given by

$$g(r) = \frac{Np(r)}{4\pi\rho r^2}. \tag{2}$$

Hear R is the average distance, σ^2 is the Debye–Waller-like disorder factor (structure variance) describing both the structural and vibrational disorder, β is the asymmetry parameter, $\Gamma(x)$ is

Euler's gamma function calculated for $x = 4/\beta^2$, n is the coordination number and ρ is the density.

3.1.1. Si atoms neighbourhood. The Si–O radial correlation is strongly peaked at the distance of 1.62 ± 0.01 Å. The value of the Debye–Waller-like factor, σ^2, for the first Si–O PDF peak, amounts typically to 0.0025 ± 0.0005 Å^2, whereas the asymmetry parameter, β, is of the order 0.5 ± 0.1. From the inspection of the O–Si–O angular distributions, peaked between 100° and 120°, with the maximum at about 110°, and the Si–O–O distributions, peaked at about 35°, it follows that the regular SiO_4 tetrahedron is the dominating structural unit in all the simulated structures. This result finds confirmation in a number of experimental works [5, 9, 10].

In our simulations over 95% of the Si atoms have tetrahedral first coordination shell. In order to characterize the SiO_4 tetrahedra we used the tetrahedricity parameters, T_1 [43] and T_2 [44]

$$T_1 = \frac{\sum_i (l_{\mathrm{O–O}} - l_{\mathrm{O–O},i})^2}{l_{\mathrm{O–O}}^2} \tag{3}$$

$$T_2 = \frac{\sum_i (l_{\mathrm{O–O}} - l_{\mathrm{O–O},i})^2}{l_{\mathrm{O–O}}^2} + \frac{\sum_i (l_{\mathrm{Si–O}} - l_{\mathrm{Si–O},i})^2}{l_{\mathrm{Si–O}}^2} \tag{4}$$

where $l_{\mathrm{O–O},i}$ and $l_{\mathrm{Si–O},i}$ are the lengths of the ith tetrahedron's O–O edge and Si–O distances, and $l_{\mathrm{O–O}}$ and $l_{\mathrm{Si–O}}$ are the average O–O and Si–O distances. The T_1 parameter estimates only the overall shape of the tetrahedra, with no reference to the position of the central cation. The newly introduced shape estimator (4) additionally takes into account deviations in the cation localization. The ideal tetrahedron is characterized by zero values of both T_1 and T_2 estimators. The T_1 values are less than 0.02 for over 90% of the SiO_4 tetrahedra obtained in our simulations, whereas the remaining percentage of the tetrahedra have their T_1 values between 0.02 and 0.04. As far as the T_2 parameter is concerned, its values do not exceed 0.02 for about 80% of the terahedra, while for most of the remaining SiO_4 units it remains in the interval 0.02 to 0.04 (a few per cent of the tetrahedra have somewhat higher T_2 values).

As mentioned above not all Si atoms in our MD-simulated samples have four-fold coordination. For about 5% of them the five-fold oxygen coordination was found. All these SiO_5 groups are rather regular triangular bi-pyramids.

3.1.2. Pb atoms neighbourhood. Figure 1 shows PDFs $g_{\mathrm{X–Y}}(r)$, related to the Pb neighbourhood in the $x\mathrm{PbO}(1-x)\mathrm{SiO}_2$ glasses, i.e. the $g_{\mathrm{Pb–O}}(r)$, $g_{\mathrm{O–O}}(r)$ functions. Table 2 contains the parameters of the first $g_{\mathrm{Pb–O}}(r)$ peak: the MD-extracted most probable Pb–O distance R_0 (the position of the maximum of the first peak), and R, σ^2, β, n from (1) and (2). The last column of the table contains our EXAFS data on pure crystalline PbO. Table 3, constructed in a similar way, refers to the $g_{\mathrm{O–O}}(r)$.

As one can see from figure 1, the first peaks of the Pb–O $g(r)$ are rather sharp, and have maxima at $R_0 = 2.30 \pm 0.01$ Å for all glass compositions. The approximation of this distribution with the Γ-like function (1) gives the average Pb–O distance R, which systematically tends to the corresponding value in pure PbO with increasing PbO concentration (table 2). For lower lead oxide contents ($x < 0.33$) the average Pb–O distance is in the range 2.40–2.47 Å, which is about 6% higher than the Pb–O distance in pure PbO. The difference in Pb–O distances between the PbO-rich ($x > 0.67$) glasses and crystalline red lead oxide amounts to 1%.

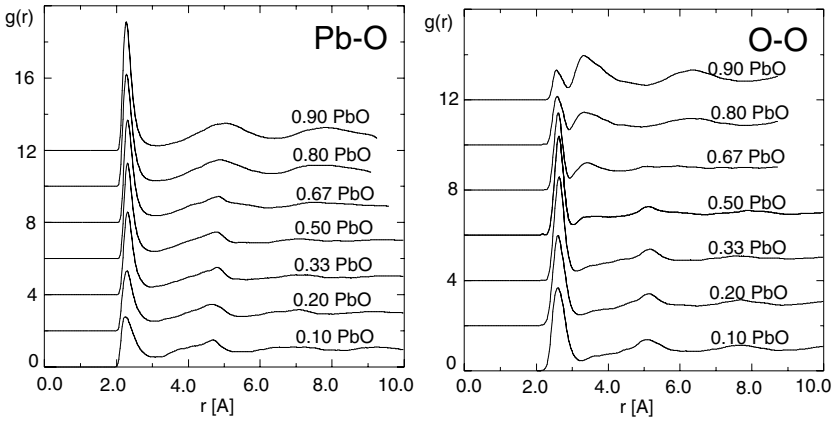

Figure 1. Pb–O and O–O pair distribution functions (PDF) in MD-simulated lead-silicate glasses. The PDFs were shifted by two from each other for clearer presentation.

Table 2. The parameters of the first Pb–O PDF peak versus PbO concentration (see text for explanation of the row labels). The R_0 values were read from the MD output files, in which the PDFs were recorded with the resolution of 0.01 Å. The fitting errors for R, σ^2, β and N were estimated to be equal to $\Delta R = 0.003$ Å, $\Delta\,\sigma^2 = 0.001$ Å^2, $\Delta\beta = 0.06$ and $\Delta N = 0.01$, respectively.

x	0.1	0.2	0.33	0.5	0.67	0.8	0.9	1.0
R_0 (Å)	2.26	2.29	2.30	2.31	2.31	2.28	2.28	2.32[a]
R (Å)	2.47	2.41	2.39	2.39	2.38	2.35	2.35	2.32
σ^2 (Å^2)	0.062	0.029	0.022	0.021	0.018	0.018	0.017	0.017
β	1.22	0.92	0.90	0.83	0.82	0.77	0.65	0.42
N	3.6	3.7	3.9	4.0	4.3	4.2	4.3	4.0

[a] From reference [40].

Table 3. The parameters of the first O–O PDF peak versus PbO concentration (see text for explanation of the row labels). The R_0 values were read from the MD output files, in which the PDFs were recorded with the resolution of 0.01 Å. The fitting errors for R, σ^2, β and N were estimated to be equal to $\Delta\,R = 0.003$ Å, $\Delta\,\sigma^2 = 0.001$ Å^2, $\Delta\beta = 0.06$ and $\Delta N = 0.01$ respectively

x	0.1	0.2	0.33	0.5	0.67	0.8	0.9	1.0
R_0 (Å)	2.60	2.60	2.64	2.62	2.62	2.58	2.56	2.81[a]
R (Å)	2.68	2.67	2.66	2.65	2.64	2.67	2.78	—
σ^2 (Å^2)	0.022	0.026	0.014	0.012	0.010	0.022	0.044	—
β	0.33	0.29	0.12	0.13	0.17	0.58	0.65	—
N	5.8	5.4	4.9	4.1	3.0	2.2	2.0	—

[a] From reference [40].

The Pb–O distance standard deviation σ^2 decreases with increasing PbO concentration from 0.062 Å^2 for $x = 0.1$–0.017 Å^2 for $x = 0.9$. The skewness parameter β has a very high value at low PbO concentrations, and decreases systematically with increasing x from 1.22 for $x = 0.1$ to 0.65 for $x = 0.9$. This means that the dispersion in the Pb–O lengths decreases with increasing PbO content.

The average coordination number for the Pb–O pair, as calculated integrating the $g(r)$ upto the minimum between the two first peaks, is somewhat higher than four for $x < 0.5$

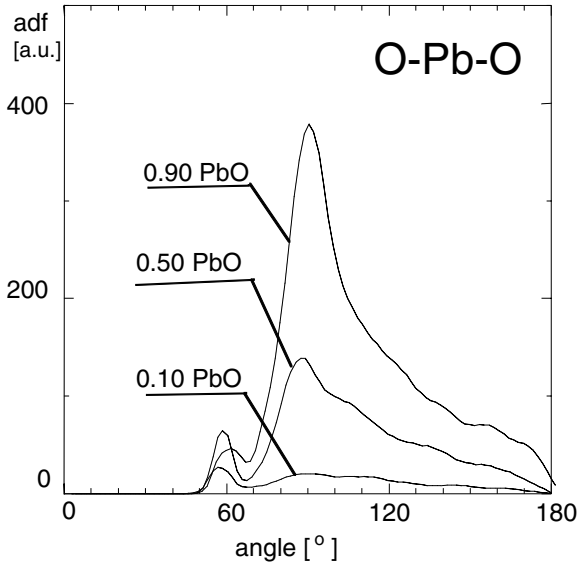

Figure 2. Angular distribution functions related to the Pb atom environment for several glass stoichiometries. Cut-off range for the Pb–O distance was equal to 3.0 Å.

and close to five for higher PbO concentrations. However, decomposing the PDF into Γ-like distributions, and integrating the first peak only, one obtains the coordination numbers listed in table 2.

Figure 2 shows the distribution of occurrences of angles between two adjacent Pb–O bonds for several glass compositions. The distributions were calculated globally over all the atoms within the simulation boxes, i.e. all the O–Pb–O triples, independent of the number of neighbouring oxygen atoms, are taken into account. The overall O–Pb–O angle distributions are peaked at 60° and 90° for all the stochiometries considered.

More detailed information on the local structure around the Pb atoms can be obtained, however, by analysing the O–Pb–O angle distributions separately for n coordinated Pb atoms. Such an analysis leads to the following conclusions. At low PbO concentrations, say $x \leqslant 0.25$, about 15% of Pb atoms have a three-fold oxygen coordination. For these three-fold configurations the distribution of the O–Pb–O angles is peaked at 120°, so the PbO_3 groups are rather flat. In the range of x from 0.33 to 0.5 about 3% of Pb atoms have three-fold oxygen coordination, and for higher PbO concentrations no PbO_3 groups have been detected. For $x \leqslant 0.5$ the PbO_4 groups dominate, whereas for $x \geqslant 0.67$ a significant fraction of Pb atoms with five oxygen neighbours appears. In the latter case, however, one of the five neighbours is more distant than the remaining four neighbours. In most of the PbO_4 groups all the oxygen atoms remain on one side of the Pb atom. Assuming that the second $g(r)$ peak of the O–O correlation (3.32 Å), which clearly appears in glasses with high PbO concentration (see figure 1), corresponds to the edge of the oxygen basal plane of the PbO_4 pyramid; the O–Pb–O angle should be 87° (figure 2). An angular distribution function for O–O–O triples, calculated for the O–O distances limited to the interval of radii somewhat higher than 3.32 Å, has a peak at about 90°, which means that the PbO_4 group with a good approximation is a square pyramid. Let us introduce the following estimator of the PbO_4 pyramid's shape [44]

$$P = \frac{\sum_i (l_{\mathrm{Pb–O}} - l_{\mathrm{Pb–O}}, i)^2}{l_{\mathrm{Pb–O}}} + \frac{\sum_i (l_{\mathrm{O–O}} - l_{\mathrm{O–O,i}})^2}{l^2_{\mathrm{O–O}}}. \tag{5}$$

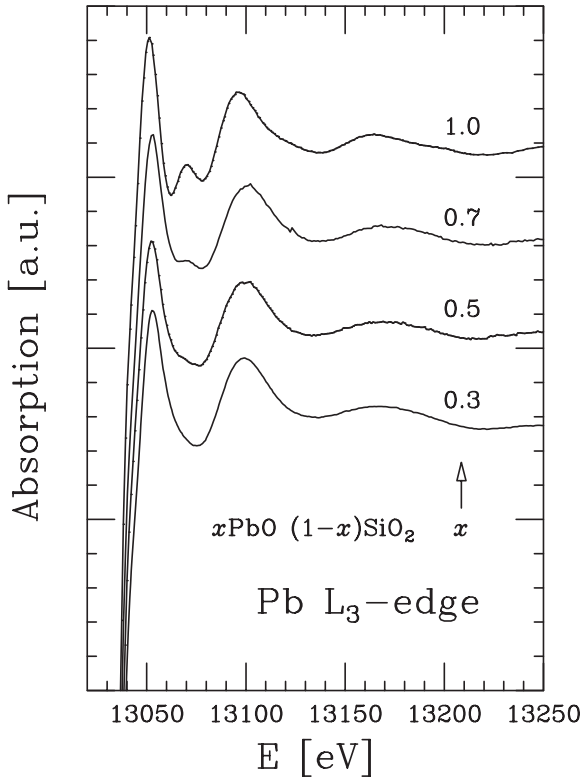

Figure 3. Comparison of the XANES spectra of lead oxide and x PbO $(1-x)$ SiO_2 glasses with $x =$ 0.7, 0.5, 0.3 (from top to bottom), recorded at the Pb L_3-edge. The spectra were shifted by 0.05 from the lower lying profile for a clear presentation.

In (5) $l_{Pb-O,i}$ is the length of the ith Pb–O edge and l_{Pb-O} is the average length of the Pb–O edges, and similarly, $l_{O-O,i}$ is the length of the ith O–O edge and l_{O-O} is the average length of the O–O edges. P values lower than 0.1 are found for about 30% of the pyramids for $x \leqslant 0.5$, and for about 70% of those in the PbO-rich samples ($x \geqslant 0.67$). The distribution of P values is significantly broader for low x's than for the high ones. Thus the PbO_4 pyramids are more regular at higher PbO contents.

3.2. EXAFS and XANES measurements

Figure 3 shows the absorption spectra of crystalline tetragonal (red) lead oxide and lead-silicate glasses with various PbO contents. One can see how the shape of the XANES region of the spectra depends on the amount of lead oxide in the sample. With decreasing x a characteristic peak of pure red lead oxide at about 13 070 eV ($k \approx 3$ Å^{-1}), which is absent in the spectrum of pure fcc lead [45], disappears gradually.

The results of the GNXAS analysis, in which we took into account only the first-shell contribution in the theoretical signal modelling, are shown in figure 4 and table 4. The bond-length probability density $p(r)$ was modelled using equation (1). Equation (1) is especially useful for studying short-range properties by using EXAFS, which is particularly sensitive to the local ordering and almost blind to the long-range correlations [17–19, 22–24]. Typical uncertainty obtained for distances using the procedure for error analysis calculated in

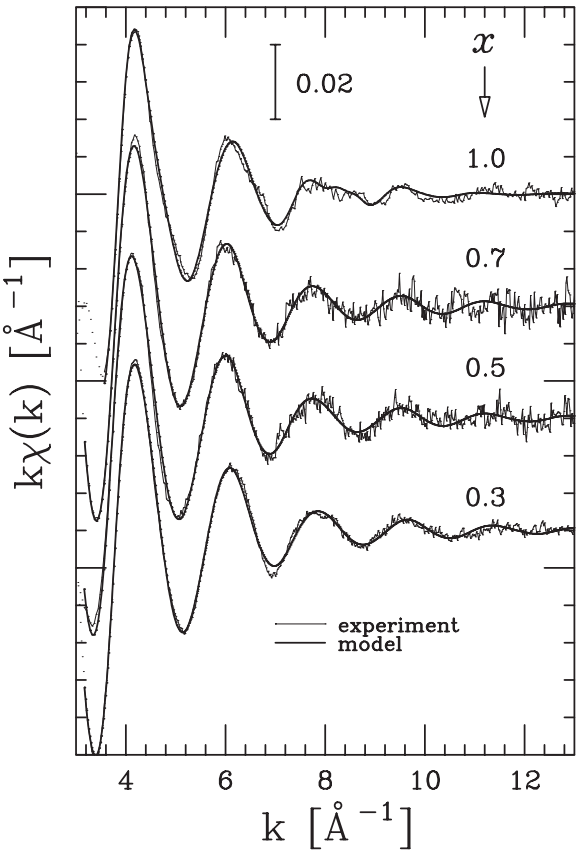

Figure 4. Comparison of the EXAFS experimental spectra (thin curve) with a calculated (thick curve) first-shell signal in the k space for pure PbO and lead-silicate glasses with $x = 0.7, 0.5, 0.3$, from top to bottom, respectively. The curves were shifted by 0.03 Å^{-1} from the lower lying profile for a clear presentation.

Table 4. Parameters of the first Pb–O PDF peak obtained from EXAFS spectra.

x	0.3	0.5	0.7	1.0
R_0 (Å)	2.28(1)	2.28(1)	2.27(1)	2.28(1)
R (Å)	2.38(1)	2.39(1)	2.38(1)	2.32(1)
σ^2 (Å^2)	0.025(3)	0.025(3)	0.025(3)	0.017(2)
β	1.0(2)	1.2(2)	1.3(2)	0.4(1)
N	4.0(3)	3.9(3)	3.9(3)	4.0(2)

95% confidence intervals in the multi-dimensional parameter space, accounting for possible correlations as described elsewhere [19, 46], is about 0.01 Å, while the absolute error on amplitude factors (i.e. N, σ^2) is of the order of 10%. The relative error on those latter parameters is much lower because we used the same amplitude reduction factor S_0^2 for all the considered samples (see section 2.3). The skewness β is also measured with a reasonable accuracy (around 20%).

As can be seen the decreasing content of lead oxide does not change the Pb–O average bond length. The same holds for the most probable Pb–O distance, which according to our analysis amounts to ∼2.28 Å, and is equal to the corresponding value for crystalline PbO. At this distance, independent of the glass composition, each Pb atom has four oxygen neighbours (N values in table 4), so the PbO_4 groups are the basic structural units of the lead subsystem in the investigated lead-silicate glasses. The exact geometry of the PbO_4 units remains unknown within our EXAFS analysis. As shown in table 4, the dispersion of the Pb–O distances is significantly higher in glasses than in pure crystalline PbO. The standard deviation increases in all of the glasses (in a covalent compound we expect that the variations of the σ^2 from the crystal to glass are due to static distortions while the vibrational amplitudes are locally unaffected). The asymmetry parameter β is three times higher in glasses than in crystalline PbO. It means that in glassy structures there is a certain fraction of deformed PbO_4 units, which can contain at least one Pb–O distance of non-typical length. In fact, the determined Pb–O coordination numbers for the glasses with $x = 0.3$, 0.5 and 0.7 do not exceed 4.0 (the Pb–O coordination number in crystalline PbO).

3.3. Comparison of MD and EXAFS results

Let us compare the molecular dynamics results obtained for $x = 0.33$, 0.5 and 0.67 with the EXAFS data obtained for glasses of similar compositions ($x = 0.3$, 0.5 and 0.7).

The most probable Pb–O distances, R_0, obtained from the MD simulations and the EXAFS measurements, in the PbO concentration range $0.3 \leqslant x \leqslant 0.70$, amount to 2.30 ± 0.01 Å and 2.28 ± 0.01 Å, respectively, and thus are identical within the distance determination errors. The same refers to the mean Pb–O distance, R (cf tables 2 and 4). The first Pb–O coordination numbers determined in the EXAFS experiment and in the MD simulations also agree within the determination uncertainty.

The σ^2 values inferred from EXAFS are about 15% and 40% higher than the corresponding values obtained from the simulations for low and high PbO concentrations, respectively. The dependence of β on x is quite different between MD and EXAFS, and the numerical values of β obtained by the two methods differ roughly by a factor of about 1.5. Despite the discrepancies in the σ^2 and β parameters, the overall shapes of the first Pb–O PDF peak are very similar (figure 5), and only the details are different, especially for high PbO concentrations. The shape of the first $g(r)$ peak depends on the interplay between three different parameters: R, σ^2 and β. The height depends on the oxygen density and coordination number. A high β results in a skewed distribution with a narrower apparent width. This explains why distributions with slightly different values of β and σ^2 are found in good qualitative agreement.

From the comparison between EXAFS-extracted and MD-simulated first PDF peaks (figure 5) we can learn that the oversimplified force field model proposed in [32] for the Pb–O interaction, used in our simulations, is not able to reproduce completely our experimental EXAFS results. Although the model of [32] allows most of the structural features of lead-silicate glasses in a wide range of stoichiometries to be reproduced in a satisfactory way, it fails in some details (the Pb–O interaction is somewhat too soft and suffers from the lack of attractive polarization interaction between the Pb^{2+} and O^{2-} ions).

3.4. Comparison with the results of previous investigations

Crystalline red PbO is built [40] from parallel layers of edge sharing square pyramids PbO_4, and the Pb–O distance is about 2.32 Å. This value is in excellent agreement with the average distance R determined from EXAFS experiment on pure PbO.

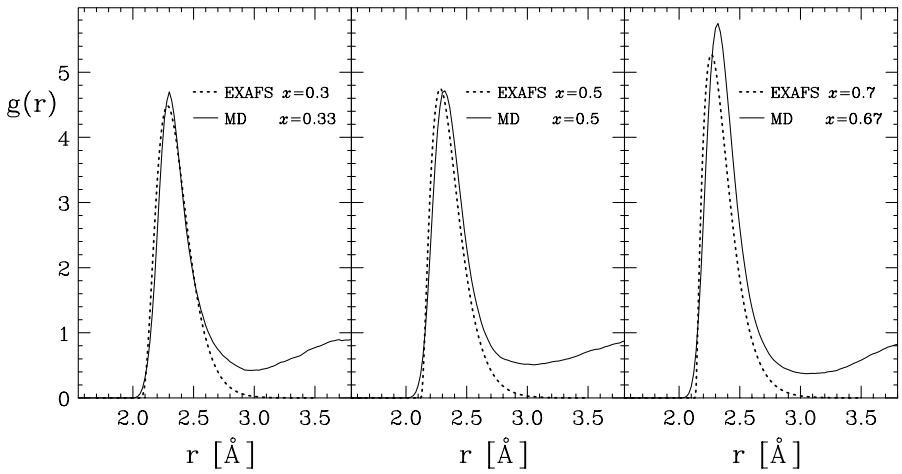

Figure 5. First-shell Pb–O peak profiles of $x\,\mathrm{PbO}(1-x)\mathrm{SiO_2}$ glasses, determined by GNXAS analysis (dashed curve) and MD simulations (solid curve). The PDFs were reconstructed using the oxygen atomic densities of 0.038 25, 0.037 57 and 0.035 663 atoms $\mathrm{Å}^{-3}$ for $x = 0.3$, 0.5 and 0.7, respectively.

According to [47], in crystalline $PbSiO_3$ one-third of the Pb atoms are coordinated by three oxygen atoms (two of them placed at a distance of 2.2–2.3 Å, and one at a distance of 2.45–2.6 Å). The remaining Pb atoms are coordinated by four oxygen atoms (two of them placed at distance of 2.2–2.3 Å, and two at the distance of 2.45–2.6 Å). The mean value of the mentioned data, 2.39 Å, agree both with our MD- and EXAFS-deduced average Pb–O distance, $R = 2.39 \pm 0.01$ Å. In crystalline $PbSiO_3$ the average oxygen coordination of Pb atom is 3.67 [47]. Our EXAFS-extracted Pb–O coordination number in glassy $PbSiO_3$ equals to 3.9 ± 0.3 (table 4).

Several authors report a four-fold oxygen coordination of Pb atoms in the considered glasses, particularly for higher PbO contents. According to [10, 48, 49], in the $x\mathrm{PbO}(1-x)\mathrm{SiO_2}$ glass with $x > 0.6$ one can find zigzag chains of square PbO_4 pyramids, interconnected by SiO_4 tetrahedra or PbO_6 octahedra. According to [8], for $0.31 \leqslant x \leqslant 0.66$, the Pb atoms have two oxygen neighbours at a distance of 2.22 Å, and two other oxygen neighbours at a distance of 2.4–2.42 Å, slightly increasing with increasing x. The increasing x results also in increasing dispersion of the second-neighbour Pb–O distances. Similar tendencies are seen also in our EXAFS-extracted data, where the increasing content of lead oxide is accompanied by a successive increase of the skewness parameter with the coordination number almost equal to 4.

On the other hand, according to the model of Imaoka and co-workers [11] (x-ray diffraction method), in the range $0.33 \leqslant x \leqslant 0.66$ the lead oxide subsystem appears in the form of $[PbO_3]_n$ chains mixed with SiO_4 tetrahedra chains, so the oxygen coordination of Pb atoms equals to 3. The predictions of the Imaoka model have been supported by neutron diffraction measurements of [12]. Our results of MD simulations and EXAFS measurements do not agree with the model proposed in [11]. Although the PbO_3 pyramids have been detected in our MD-simulated structures (particularly at rather low PbO concentrations), they cannot be treated as the only, or even the dominating fundamental structural units. Instead, the suggestions that the PbO_4 square pyramids dominate in the considered glasses [4, 9, 10, 48, 49], have been fully confirmed in our work. The co-existence of the PbO_3 and PbO_4 pyramids, which we have found in the MD-simulated glass structures at low PbO concentrations, was previously suggested in [7, 47, 50].

4. Medium-range order

Since the EXAFS experiment probes the local atom environment within rather short ranges, it is difficult to extract much information from it on the medium-range ordering. The only, quite obvious, conclusion from our XAS measurements is that with decreasing lead oxide content the Pb structural units become more and more distant from each other. The strong decrease of the 13 070 eV peak (figure 3), coming from the ordered PbO to the glass with $x = 0.3$, is related to the presence of disorder at the medium-range level. The complete disappearance of this peak for low PbO concentrations could be related to the lack of connectivity between two successive PbO_4 structural units.

However, having obtained a good agreement of our simulation results with experimental data for the short-range order, and correct system densities in zero external pressure simulations, we expect that the simulated structures should also reveal a reasonable spatial ordering of the structural units. So we analysed in detail the medium-range order in our MD-simulated samples.

The medium-range order in the MD-simulated glasses was investigated mainly by cation–anion ring analysis. A closed chain of bonded atoms, consisting of N cations and N anions, is called an N-member ring [51, 52]. We say that its length equals N. The ring analysis has been performed as follows.

At first, the full neighbours list (FNL) for all the atoms of given kinds (i.e. Si and O, and Pb and O), were constructed, according to a simple adjacency criterion (user-defined cut-off radius), and taking into account the periodic boundary conditions. The FNL defines a graph, which represents atoms and interatomic bonds. In general, the obtained graph does not need to be connected. Thus before further data analysis the full bonding graph was split into separate connected sub-graphs. In order to minimize the execution time and the memory request from the main program (ring calculation), from the adjacency sub-graphs were eliminated all the dangling structures, i.e. all the atoms which do not belong to any ring or path between rings. Then, the ring basis was determined for each connected graph using the program based on our algorithm mentioned in section 2.1. As the result we obtained full information on basal rings (node numbers) and ring length statistic. The concrete set of basal (linearly independent) rings for a given graph depends only on the node enumeration (the base is not unique), but the length distribution is of course unique. In our calculations of basal rings no approximations are made. The quality of the physical results depends entirely on the input atom configuration, i.e. practically on the interaction model used in the MD simulations. Having identified all the basal rings, their geometrical properties and length distribution can be readily analysed. Moreover, the eliminated dangling structures were also submitted to a statistical analysis (distribution of their lengths, density of bifurcations, etc, see [27, 29]). It should be noted that, due to the periodic boundary conditions, usually several spurious long (up to $N = 50$ for several compositions) rings are found. These can be easily identified and disregarded in the further analysis. Let us discuss in turn the SiO_2 and PbO subsystems.

4.1. The Si–O–Si–O– · · · rings

The Si–O adjacency graphs, for which the ring analysis was performed, were constructed under the condition that the Si–O distance was shorter than 2 Å. The results of the analysis can be summarized as follows.

Three different intervals of PbO concentrations can be distinguished: $x \leqslant 0.33$, $0.4 \leqslant x \leqslant 0.5$ and $x \geqslant 0.67$. In these intervals the Si–O–Si–O– · · · rings have different properties:

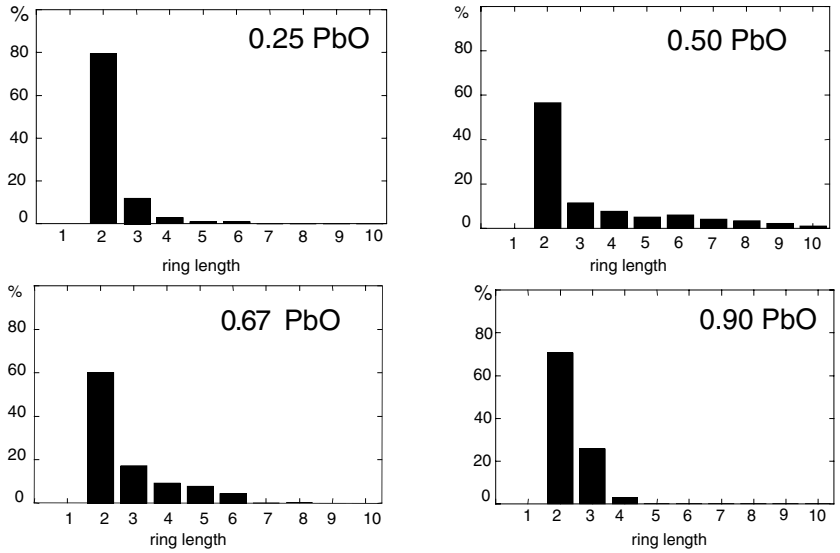

Figure 6. The Pb–O–Pb–O $\cdots$ ring statistics in lead-silicate glasses with $x = 0.25$, 0.5, 0.67 and 0.90. The lead–oxygen adjacency graph was constructed with the cut-off radius for the Pb–O distance equal to 3.0 Å.

- For $x \leqslant 0.33$ the graphs are fully connected and contain all the Si and O atoms. The SiO_2 subsystem in this x-range is built mainly from five- and six-member rings. No two-member rings (corresponding to edge sharing tetrahedra) are present. With increasing x the percentage of long rings increases, however their length does not exceed 10.
- For $x = 0.4$, 0.45 and 0.5, the biggest connected graphs in our MD-simulated structures contained about 99%, 93% and 91% of Si and O atoms, respectively (the remaining Si and O atoms belonged to isolated SiO_4 or Si_2O_7 groups, forming stars and bi-stars, respectively). In these biggest connected adjacency graphs, about 35%, 50% and 80% of atoms belonged to dangling structures, i.e. bifurcated chains (trees). In other words, for $x = 0.4$, 0.45 and 0.5 only 65%, 50% and 20% of all Si and O atoms, respectively, belonged to some ring. Moreover, as much as about 20% of all rings had lengths from 10 to 20 (i.e. contained 20–40 atoms). On the basis of the cited numerical data one can conclude that the SiO_2 subsystem loses its three-dimensional connectivity at $x \approx 0.45$. A similar loss of the SiO_2 system connectivity at $x \approx 0.45$ was previously reported in [9].
- For PbO concentrations $x \geqslant 0.67$ the full adjacency graph is highly disconnected and consists practically of only five- and nine-node groups, identified to be isolated SiO_4 stars or Si_2O_7 bi-stars.

4.2. The Pb–O–Pb–O $\cdots$ rings

In the adjacency graph construction, the Pb and O atoms were considered bonded if their distance was less than 3.0 Å (the approximate position of the first minimum of the Pb–O pair distribution function). Examples of length statistics of linearly independent (basal) Pb–O–Pb–O $\cdots$ rings (for $x = 0.25$, 0.5, 0.67 and 0.9) are shown in figure 6.

For $x \leqslant 0.2$ the Pb–O adjacency graph splits into many connected sub-graphs, representing isolated short O–Pb–O– $\cdots$ linear chains or structures containing 1 or 2 two-member Pb–O

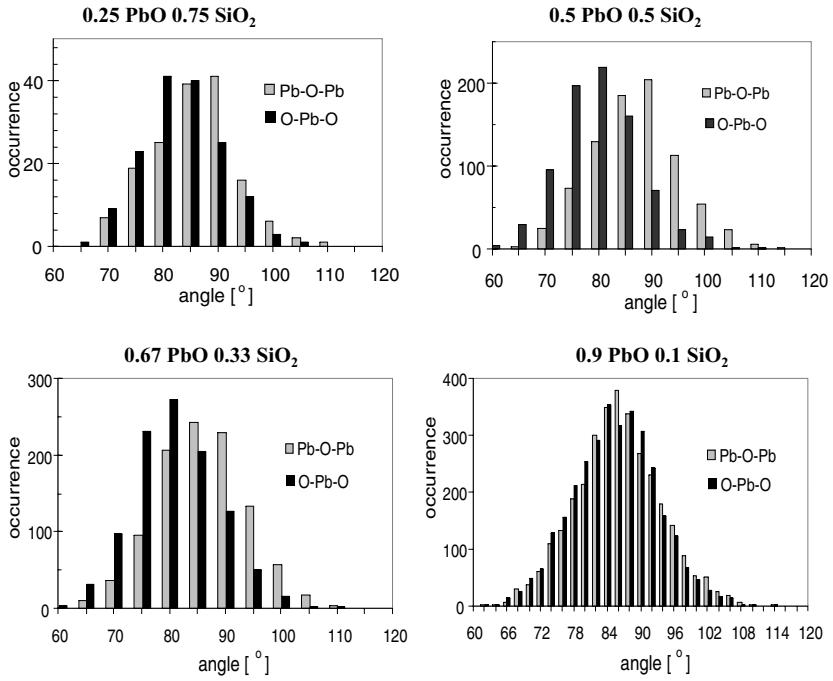

Figure 7. Angular distribution functions (ADF) calculated over two-member Pb–O rings for several glass composition. The cut-off radius for the Pb–O distance was equal to 3.0 Å.

rings. The first histogram in figure 6 refers to $x = 0.25$. For this PbO concentration, two larger, separated sub-graphs were detected within the simulation box: one containing 527 atoms and the other containing 191 atoms (despite several small sub-graphs, containing up to 10 atoms). The distribution of the ring lengths in figure 6 was calculated for the 527 atom subgraph. The corresponding distribution over the smaller graph is, however, very similar. The domination of two-member rings is clearly seen. Obviously, with increasing x the size of the maximum connected Pb–O adjacency sub-graph increases. At a PbO content as low as 0.33 more than 90% of Pb atoms in the simulation box enter formally a single connected graph. However, the structure still consists of two main sub-graphs, interconnected by linear Pb–O chains. Thus, the ring basis contains rings with a relatively wide distribution of lengths. With further increasing x, the two-, and three-member rings become systematically more frequent, whereas longer basal rings disappear completely for $x > 0.67$ (figure 6).

From the analysis of the angle distributions within the dominating two-member Pb–O rings comes the result that the PbO_4 units share their O–O edges. The angular distribution functions for O–Pb–O and Pb–O–Pb triples calculated over dominating two-member rings are shown in figure 7. As seen, the O–Pb–O and Pb–O–Pb angle distributions are similar for all glass compositions, and peaked in the range 80°–90° . All the distributions are rather wide, and somewhat shifted one from the other (figure 7). However, the distribution of sums of the inter-bond angles along the two-member rings is sharply peaked between 355° and 360° . The typical distances between the middles of the Pb-Pb and O–O diagonals do not exceed 0.5 Å, so the two-member lead–oxygen rings are rather flat. This means that the mutual configuration of adjacent edge sharing PbO_4 pyramids in crystalline red PbO ($P4/nmm$ space group) is rather well preserved in lead-silicate glasses [40].

5. Conclusions

We have performed extensive MD simulations of lead-silicate glasses $x\mathrm{PbO}(1-x)\mathrm{SiO}_2$ in a wide range of compositions, $x = 0.1$–0.9, and the EXAFS measurements for glasses of three different stoichiometries. The obtained numerical and experimental results are compatible.

From our investigations on the short-range structure (EXAFS and MD) the results are:

(1) the Pb–O average distance is independent of the glass composition ($x > 0.3$), and agrees with the previously published results of other authors [5, 8, 49];
(2) the PbO_4 group is a dominant structural unit in the considered glasses, in agreement with [4, 9, 10, 48, 49].

Encouraged by the good agreement of our simulation results with experimental data for the short-range order, we analysed in detail the medium-range order in our MD-simulated samples. The cation–anion ring analysis was used. It turned out that:

(1) the connectivity of the SiO_4 tetrahedra corner-sharing network breaks at about $x = 0.45$;
(2) the Pb structural units form a continuous network even at relatively low PbO concentration ($x \geqslant 0.25$). Since the two-member rings dominate, the network consists mainly of edge sharing polyhedra. The analysis of distributions of O–Pb–O and Pb–O–Pb angles along two-member rings give the result that the relative orientation of two adjacent PbO_4 pyramids is similar to that in crystalline red PbO.

Acknowledgments

The opportunity to perform our MD simulations at the TASK Computer Centre (Gdansk, Poland) is gratefully acknowledged. The work has been partially sponsored by KBN, grant 7 T08D 009 20.

References

[1] Wang C C 1970 *Phys. Rev.* B **2** 2045
[2] Wiza J L 1979 *Nucl. Instrum. Methods* **62** 587
[3] Trzebiatowski K, Murawski L, Koscielska B, Chybicki M, Gzowski O and Davoli I 1997 *Proc. Conf. on Fundamentals of Glass Science and Technology (Vaxjo, Sweden*)
[4] Warrel C A and Henshall T 1978 *J. Non-Cryst. Solids* **29** 283
[5] Verweij H and Konijnendijk W L 1976 *J. Am. Ceram. Soc.* **11/12** 517
[6] Zahra A M and Zahra C Y 1993 *J. Non-Cryst. Solids* **155** 45
[7] Fayon F, Bessada C, Massiot D, Farnan I and Coutures J P 1998 *J. Non-Cryst. Solids* **232/234** 403
[8] Fayon F, Landron C, Sakurai K, Bessada C and Massiot D 1999 *J. Non-Cryst. Solids* **243** 39
[9] Wang P W and Zhang L 1996 *J. Non-Cryst. Solids* **194** 129
[10] Morikawa H, Takagi Y and Ohno H 1982 *J. Non-Cryst. Solids* **53** 173
[11] Imaoka M, Hasegawa H and Yasui I 1986 *J. Non-Cryst. Solids* **85** 393
[12] Yamada K, Matsumoto A, Niimura N, Fukunaga T, Hayashi N and Watanabe N 1986 *J. Phys. Soc. Japan* **55** 831
[13] Suzuya K, Price D L, Saboungi M-L and Ohno H 1997 *Nucl. Instum. Methods* B **133** 57
[14] Masteraro V R, Zanotto E D, Lequeux N and Cortès R 2000 *J. Non-Cryst. Solids* **262** 191
[15] Hockney R W and Eastwood J W 1987 *Computer Simulation using Particles* (New York: McGraw-Hill)
[16] Rapaport D C 1995 *Art of the Molecular Dynamics Simulation* (Cambridge: Cambridge University Press)
[17] Koningsberger D C and Prins R (ed) 1988 *X-Ray Absorption-Principles, Applications, Techniques of EXAFS SEXAFS and XANES* (New York: Wiley)
[18] Filipponi A, Di Cicco A, Tyson T A and Natoli C R 1991 *Solid State Commun.* **78** 265
[19] Filipponi A, Di Cicco A and Natoli C R 1995 *Phys. Rev.* B **52** 15 122
Filipponi A, Di Cicco A and Natoli C R 1995 *Phys. Rev.* B **52** 15 135

[20] Rybicki J, Alda W, Rybicka A and Feliziani S 1996 *Comput. Phys. Commun.* **97** 191
[21] Rybicka A, Chybicki M, Laskowski R, Alda W and Feliziani S 1997 *Gdansk 97: Proc. 4th Int. Conf. on Intermolecular Interaction in Matter* p 42
[22] Filipponi A 1994 *J. Phys.: Condens. Matter* **6** 8415
[23] D'Angelo P, Di Nola A, Filipponi A, Pavel N V and Roccatano D 1994 *J. Chem. Phys.* **100** 985
[24] Di Cicco A, Rosolen M J, Marassi R, Tossici R, Filipponi A and Rybicki J 1996 *J. Phys.: Condens. Matter* **8** 10779
[25] Mancini G 1997 *TASK Quart.* **1** 89
[26] Mancini G 2001 *Comput. Phys. Commun.* submitted
[27] Bergmański G, Rybicki J and Mancini G 2000 *TASK Quart.* **4** 555
[28] Rybicki J, Bergmański G and Mancini G 2001 *J. Non-Cryst. Solids* submitted
[29] www.task.gda.pl/software
[30] Andersen H C 1980 *J. Chem. Phys.* **72** 2384
[31] Kolafa J and Perram J W 1992 *Mol. Simul.* **9** 351
[32] Damodaran K V, Rao B G and Rao K J 1990 *Phys. Chem. Glasses* **31** 212
[33] Rybicka A 1999 *PhD Thesis* Technical University of Gdansk, Gdansk
[34] Balducci R and Pearlman R S 1994 *J. Chem. Inf. Comput. Sci.* **34** 822
[35] Di Cicco A and Filipponi A 1994 *Phys. Rev.* B **49** 12564
[36] Filipponi A 1995 *Physica* B **208/209** 29
[37] Filipponi A and Di Cicco A 2000 *TASK Quart.* **4** 575
[38] Di Cicco A, Stizza S., Filipponi A, Boscherini F and Mobilio S. 1992 *J. Phys. B: At. Mol. Opt. Phys.* **25** 2303
[39] Tyson T A, Hodgson K O, Natoli C R and Benfatto M 1992 *Phys. Rev.* B **46** 5997
[40] Wyckoff R W G 1964 *Crystal Structures* (New York: Wiley–Interscience)
[41] Laskowski R and Rybicki J 2000 *Phys. Status Solidi* (b) **217** 737
[42] Filipponi A and Di Cicco A 1995 *Phys. Rev.* B **51** 12322
[43] Medvedev N N and Naberukhin Y I 1987 *J. Non-Cryst. Solids* **94** 402
[44] Rybicki J, Witkowska A, Bergmanski G, Bosko J, Mancini G and Feliziani S 2001 *Comput. Met. Sci. Technol.* at press
[45] Witkowska A, Rybicki J, Trzebiatowski K, Di Cicco A and Minicucci M 2000 *J. Non-Cryst. Solids* **276** 19
[46] Filipponi A 1995 *J. Phys.: Condens. Matter* **7** 9343
[47] Boucher M L and Peacor D R 1968 *Z. Kristallogr.* **126** 98
[48] Mydlar M, Kreidl N, Hendren J and Clayton G 1970 *Phys. Chem. Glasses* **11** 196
[49] Smets B M J and Lommen T P A 1982 *J. Non-Cryst. Solids* **48** 423
[50] Hosono H, Kawazoe H and Kanazawa T 1982 *Yogyo-Kyokai-Shi* **88** 141
[51] Elliott R 1995 *J. Non-Cryst. Solids* **182** 1
[52] Hamann D R 1997 *Phys. Rev.* B **55** 14 784